

# TDOA-Based Localization Using Interacting Multiple Model Estimator and Ultrasonic Transmitter/Receiver

Rui Zhang, Fabian Höflinger, and Leonhard Reindl, *Member, IEEE*

**Abstract**—This paper presents a novel indoor localization system using a self-built ultrasonic transmitter and a receiver. In comparison to commercial localization systems, our ultrasonic system is more robust against multipath propagation at indoor conditions and provides accurate time difference of arrival measurements. Besides, by improving the coverage of our ultrasonic system, the number of system components is significantly reduced. The actual position of the target is then determined by interacting multiple model estimator, which offers protection against the measurement noise at both line-of-sight and non-line-of-sight conditions through simultaneous running of extended Kalman filter and robust extended Kalman filter. The experimental results shows that our system is able to deliver the localization solution with higher accuracy compared to commercially available options.

**Index Terms**—Indoor localization, interacting multiple model (IMM), Kalman filter, M-estimator, time difference of arrival (TDOA), ultrasound.

## I. INTRODUCTION

ALTHOUGH localization is becoming available to the general public and businesses via a widespread use of global positioning system (GPS) receivers, the GPS signal may not be available in indoor areas. Furthermore, the achieved accuracy of GPS localization is usually not sufficient. It can be a significant problem in certain situations to provide an accurate position estimate of mobile station (MS).

Wireless network infrastructure-based localization systems being an alternative solution use existing wireless communication network infrastructures to determine the geographical location of an MS. Mobile indoor positioning based on such systems is used to provide various location-based services, such as hostage rescue, emergency service, location-based billing, fleet management, and intelligent transport systems.

Manuscript received July 13, 2012; revised November 16, 2012; accepted November 30, 2012. Date of publication May 1, 2013; date of current version July 10, 2013. This work was supported by the German Research Foundation (DFG) within the Research Training Group 1103 (Embedded Microsystems). This paper was presented in part at the IEEE 9th International Multi-Conference on Systems, Signals and Devices (SSD), Chemnitz, Germany, 2012 [1]. The Associate Editor coordinating the review process was Dr. M. Yeary.

The authors are with the Department of Microsystems Engineering, University of Freiburg, Freiburg 79110, Germany (e-mail: rui.zhang@imtek.uni-freiburg.de; fabian.hoeflinger@imtek.uni-freiburg.de; reindl@imtek.uni-freiburg.de).

Color versions of one or more of the figures in this paper are available online at <http://ieeexplore.ieee.org>.

Digital Object Identifier 10.1109/TIM.2013.2256713

The MS can be located by measuring the parameters of its signals received at a fixed set of base stations (BSs). In order to achieve the accuracy standard and performance requirement by the Federal Communication Commission, different measurement approaches such as angle of arrival, time of arrival (TOA)/run trip time of arrival (RTT), and time difference of arrival (TDOA) received signal strength or the combination of these methods can be utilized [2].

Several wireless network (WLAN) infrastructure-based indoor localization systems and approaches are available. Most of them are optical systems which are able to achieve high precision in indoor environments [3]. However, most commercially available systems are expensive [4]. Other tracking systems working with radio frequencies in different frequency bands are cheap. However, these systems can only deliver a positioning accuracy between 2 and 3 m in indoor environments [5]. Besides, the multipath propagation of radio waves also disturbs the measurement results [6].

Our approach to track an MS in indoor environments relies on an ultrasound localization system [1]. We use the ultrasound to estimate the distance between installed receivers and a mobile transmitter; thus, multipath propagation can be detected due to its slow speed. Besides, ultrasound is more robust to noise interruption due to its particular frequency. Priyantha [7] used these characteristics to develop a CRICKET ultrasound system. We modified the CRICKET system by using different algorithms and improving the coverage range. Compared with the CRICKET system, our transmitter is able to cover a direction of 360°; thus, only one transmitter is needed [8]. Furthermore, we implemented a WLAN communication for synchronizing the receivers and therefore reducing the installation effort.

The reason why we choose TDOA instead of RTT/TOA is to lower the system complexity and achieve high measurement accuracy. Although RTT/TOA requires no synchronization and does not manipulate the measured distances, extra filter, wireless communication elements, and additional receiver transducer have to be added to the MS since the system needs to receive the ultrasonic signal or transmit a timestamp. Thus, the weight and the size of the system increase and power consumption becomes higher due to the nonexisting sleep modes. Besides, since the ultrasound speed is not very high and only one signal can be received by the MS, the different receiving times will result in a position error.

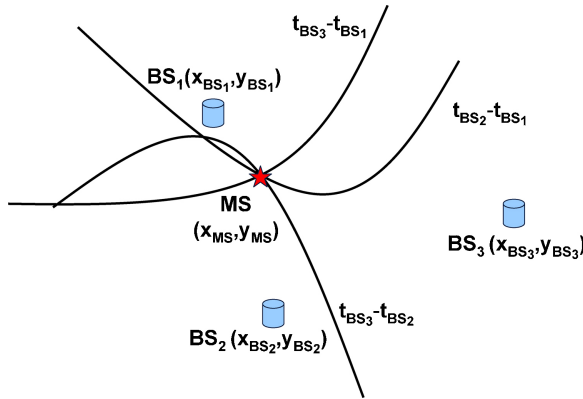


Fig. 1. TDOA hyperbolic positioning.

If the line-of-sight (LOS) path or identical bias between the MS and the BSs exists, high accuracy of positioning can be achieved due to the noise-free TDOA measurements. However, the condition of LOS path or identical bias cannot always be met since the ultrasonic signal of any path may be hidden or reflected by obstacles. Therefore, TDOA measurements can suffer from the non-line-of-sight (NLOS) path, which results in a bias in the TDOA measurement or in the worst case no TDOA measurements. Therefore, to find an algorithm that alleviates the impact of NLOS error is important.

In this paper, a novel TDOA-based localization system using ultrasonic system and interacting multiple model (IMM) estimator is presented. The system was experimentally verified in an indoor environment. The problem of NLOS interference was eliminated and the correct trajectory of an MS was successfully delivered.

The remainder of this paper is structured as follows. In Section II, the geometric description of TDOA estimation is presented. In Section III, the extended Kalman filter (EKF) estimator, robust extended Kalman filter (REKF) estimator, and IMM as the system algorithm are presented. Section IV shows the self-built ultrasonic system including a transmitter and a receiver. The experimental results and discussions are presented in Section V. Conclusion and future work are given in Section VI.

## II. GEOMETRIC DESCRIPTION OF TDOA ESTIMATION

TDOA is an observer measuring the TDOA [9], which can be converted into distance using the velocity of the ultrasound  $v_{us}$ . For stationary MS approaches, at least three BSs are required for computing MS's position, while one of the BSs is used as a reference. If there is no prior knowledge available for choosing the right intersection point, at least four BSs are required. TDOA measurements  $h_{ij}$  ( $i, j = 1, 2, 3$ ,  $i \neq j$ ) between BS $_i$  and BS $_j$  can be calculated by

$$\begin{aligned} h_{ij} &= \sqrt{(x_{BS_i} - x_{MS})^2 + (y_{BS_i} - y_{MS})^2} + v_i \\ &- \sqrt{(x_{BS_j} - x_{MS})^2 + (y_{BS_j} - y_{MS})^2} - v_j \\ &= v_{us} \times (t_{BS_i} - t_{BS_j}). \end{aligned} \quad (1)$$

From (1), the difference of two TOA measurement noises  $v_i$  ( $i = 1, 2, 3$ ) is considered to be the TDOA measurement noise. If the measured distance of the reference BS and the measured distance of rest BSs have an identical bias, there is no bias existing in the TDOA measurement and better performance can be achieved [10]. Note that any BS can be the reference BS.

## III. POSITIONING ALGORITHM

### A. EKF Estimator

The Kalman filter has been widely studied and applied in positioning due to its low computational complexity which is well suited to small mobile devices. The Kalman filter is a set of mathematical equations that provides an efficient computational (recursive) means to estimate the state of process, meanwhile minimizing the mean of the squared error [11]. Since we utilize the TDOA approach, the measurement equation is non-linear. Therefore, EKF is used to estimate the state by linearizing the measurement equation. The signal model consists of two equations.

#### 1) Process equation

$$\mathbf{x}_k = \mathbf{Ax}_{k-1} + \mathbf{Gw}_{k-1} \quad (2)$$

#### 2) Measurement equation

$$\mathbf{z}_k = h(\mathbf{x}_k) + \mathbf{v}_k. \quad (3)$$

The state vector being estimated as  $\mathbf{x}_k = [x_k \ y_k \ v_{x,k} \ v_{y,k}]^T$  contains the position and the velocity of the MS.  $\mathbf{z}_k$  is the TDOA measurement vector at the time step  $k$ ;  $\mathbf{w}_k$  and  $\mathbf{v}_k$  are the process and measurement noises. The process noise is assumed to be an independent, white Gaussian random variable

$$\mathbf{w} \sim \mathcal{N}(0, \mathbf{Q}) \quad (4)$$

where  $\mathbf{Q}$  is the process noise error covariance. In the LOS environment, measurement noise  $\mathbf{v}_k$  is assumed to be normally distributed

$$\mathbf{v}_k \sim \mathcal{N}(0, \mathbf{R}_{\text{LOS}}). \quad (5)$$

Here, the random force model is chosen as our process model [2]; therefore, the matrices in (2) are given as

$$\mathbf{A} = \begin{bmatrix} 1 & 0 & dt & 0 \\ 0 & 1 & 0 & dt \\ 0 & 0 & 1 & 0 \\ 0 & 0 & 0 & 1 \end{bmatrix}, \quad \mathbf{G} = \begin{bmatrix} dt^2/2 & 0 \\ 0 & dt^2/2 \\ dt & 0 \\ 0 & dt \end{bmatrix} \quad (6)$$

where  $dt$  is the time step duration.

The function  $h(\mathbf{x}_k)$  can be approximated using the first-order Taylor expansion about the predicted state estimate  $\hat{\mathbf{x}}_k^-$ , given in the following equation [12]:

$$h(\mathbf{x}_k) = h(\hat{\mathbf{x}}_k^-) + \frac{\partial h(\hat{\mathbf{x}}_k^-)}{\partial \mathbf{x}} (\mathbf{x}_k - \hat{\mathbf{x}}_k^-) = h(\hat{\mathbf{x}}_k^-) + \mathbf{H}_k (\mathbf{x}_k - \hat{\mathbf{x}}_k^-) \quad (7)$$

where  $\mathbf{H}_k$  is the Jacobian matrix of the partial derivatives of  $h$  with respect to  $\mathbf{x}$  at the time step  $k$ .

EKF equations are shown below, consisting of two groups: one for time update and another one for measurement update.

1) *EKF time update equations*

$$\hat{\mathbf{x}}_k^- = \mathbf{A}\hat{\mathbf{x}}_{k-1} \quad (8)$$

$$\mathbf{P}_k^- = \mathbf{A}\mathbf{P}_{k-1}\mathbf{A}^T + \mathbf{G}\mathbf{Q}_{k-1}\mathbf{G}^T \quad (9)$$

where  $\mathbf{P}_k^-$  and  $\mathbf{P}_k$  are *a priori* (predicted) and *a posteriori* (corrected) error covariances.

2) *EKF measurement update equations*

$$\mathbf{K}_k = \mathbf{P}_k^- \mathbf{H}_k^T (\mathbf{H}_k \mathbf{P}_k^- \mathbf{H}_k^T + \mathbf{R}_k)^{-1} \quad (10)$$

$$\hat{\mathbf{x}}_k = \hat{\mathbf{x}}_k^- + \mathbf{K}_k(\mathbf{z}_k - h(\hat{\mathbf{x}}_k^-)) \quad (11)$$

$$\mathbf{P}_k = (\mathbf{I} - \mathbf{K}_k \mathbf{H}_k) \mathbf{P}_k^- \quad (12)$$

where  $\mathbf{R}_k$  is the measurement noise covariance. In the LOS case,  $\mathbf{R}_k = \mathbf{R}_{\text{LOS}}$ . The term  $\mathbf{z}_k - h(\hat{\mathbf{x}}_k^-)$  is called innovation. The Kalman gain  $\mathbf{K}$  is the innovation weighting coefficient which determines the influence of the innovation in updating the estimate [11].

### B. REKF Estimator

Since EKF is accurate for problems with small non-linearities and nearly Gaussian noise statistics, its performance degrades when these conditions are not fulfilled. However, in practical positioning, large non-linearities and large outliers are normal occurrences due to the multipath and NLOS signals. In order to improve the robustness of EKF, the weighted least-squares regression form of Kalman filter using Huber's M-estimator is presented.

1) *EKF in Regression*: In order to enhance the performance of the conventional EKF and add in a robust manner, (8), (9) and (10)–(12) are firstly transformed to the form of least squares, which are shown as follows.

Recall the linearization of  $h(\cdot)$  and rewrite (2) and (3) as

$$\begin{bmatrix} \mathbf{I} \\ \mathbf{H}_k \end{bmatrix} \mathbf{x}_k = \begin{bmatrix} \hat{\mathbf{x}}_k^- \\ \hat{\mathbf{z}}_k \end{bmatrix} + \mathbf{E}_k \quad (13)$$

where  $\hat{\mathbf{z}}_k$  is defined by

$$\hat{\mathbf{z}}_k = \mathbf{z}_k - h(\hat{\mathbf{x}}_k^-) + \mathbf{H}_k \hat{\mathbf{x}}_k^- \quad (14)$$

and  $\mathbf{E}_k$  is given by

$$\mathbf{E}_k = \begin{bmatrix} \mathbf{A}(\mathbf{x}_{k-1} - \hat{\mathbf{x}}_{k-1}^-) + \mathbf{G}\mathbf{w}_{k-1} \\ -\mathbf{v}_k \end{bmatrix} \quad (15)$$

$$E\{\mathbf{E}_k \mathbf{E}_k^T\} = \begin{bmatrix} \mathbf{P}_k^- & 0 \\ 0 & \mathbf{R} \end{bmatrix} = \mathbf{S}_k \mathbf{S}_k^T \quad (16)$$

where  $\mathbf{P}_k^-$  is given by (9) and  $\mathbf{S}$  can be obtained by the Cholesky decomposition [13]. Multiplying (13) by  $\mathbf{S}_k^{-1}$ , we get

$$\mathbf{Y}_k = \mathbf{N}_k \mathbf{x}_k + \xi_k \quad (17)$$

where

$$\mathbf{N}_k = \mathbf{S}_k^{-1} \begin{bmatrix} \mathbf{I} \\ \mathbf{H}_k \end{bmatrix}, \quad \xi_k = -\mathbf{S}_k^{-1} \mathbf{E}_k, \quad \mathbf{Y}_k = \mathbf{S}_k^{-1} \begin{bmatrix} \hat{\mathbf{x}}_k^- \\ \hat{\mathbf{z}}_k \end{bmatrix}. \quad (18)$$

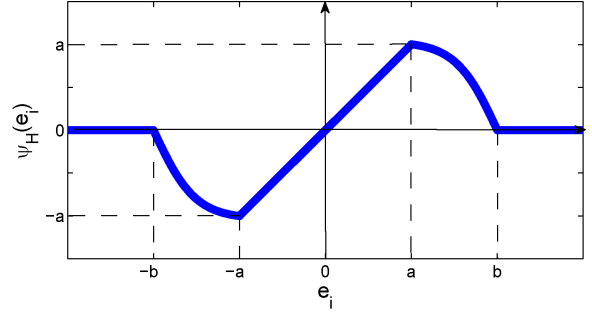


Fig. 2. Huber's minimax redescending.

Now, (17) is in the form of a standard linear least-squares regression problem with  $E\{\xi_k \xi_k^T\} = \mathbf{I}$ .

The least-squares estimator is given by

$$\hat{\mathbf{x}}_k = (\mathbf{N}_k^T \mathbf{N}_k)^{-1} \mathbf{N}_k^T \mathbf{Y}_k. \quad (19)$$

2) *Huber's M-Estimator*: According to a previous study [14], the least-squares estimates can behave badly when the error distribution is not normal, particularly when the errors are heavy-tailed. The M-estimator is used here to solve (19) in a robust manner. Note that for simplicity in the notations, the time index  $k$  is ignored in  $\mathbf{x}$ ,  $\mathbf{N}$ , and  $\mathbf{Y}$ , even though they are in fact different at each time step. The general M-estimator minimizes the objective function  $J_n$

$$\hat{\mathbf{x}} = \arg \min J_n, \quad J_n = \sum_{i=1}^n \rho(e_i) \quad (20)$$

where  $e_i = y_i - \mathbf{n}_i^T \hat{\mathbf{x}}$  and function  $\rho(\cdot)$  gives the contribution of each  $e_i$  to the objective function,  $y_i$  is the  $i$ th element of  $\mathbf{Y}$ , and  $\mathbf{n}_i^T$  is the  $i$ th row of  $\mathbf{N}$ .  $n$  is the dimension of  $\mathbf{Y}$  in (17).

Let  $\psi(\cdot) = \rho'(\cdot)$ , the influence function, be the derivative of  $\rho$ . Differentiating the objective function with respect to the coefficients  $e_i$  and setting the partial derivative to 0

$$\sum_{i=1}^n \mathbf{n}_i^T \psi(e_i) = 0. \quad (21)$$

Defining the weight function  $w(e_i) = \frac{\psi(e_i)}{e_i}$ . Then

$$\sum_{i=1}^n \mathbf{n}_i^T w(e_i) = 0. \quad (22)$$

Here, the redescending function is chosen for REKF in order to suppress the impact of noise with heavy-tailed distributions efficiently in NLOS environments. Its influence function is defined by

$$\psi_{\text{HR}}(e_i) = \begin{cases} e_i & , |e_i| < a \\ c \cdot \tanh[\frac{c(b-x)}{2}] & , a \leq |e_i| < b \\ 0 & , |e_i| \geq b \end{cases} \quad (23)$$

where  $a$  and  $b$  are clipping points and  $c$  is determined so that  $\psi_{\text{HR}}$  is continuous. Smaller values of  $a$  and  $b$  lead to a more robust estimation, but at the expense of lower efficiency when the errors are normally distributed. Generally, the clipping point is picked to give reasonably high efficiency in the normal-distributed case. However, in our case, REKF will be

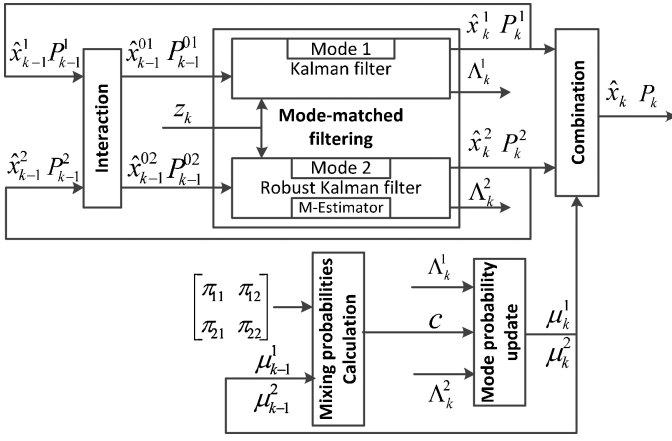


Fig. 3. IMM structure.

only used to minimize the impact of the NLOS propagation when applying the IMM estimator; therefore, smaller values are chosen for clipping points:  $a = 1\sigma$  and  $b = 4\sigma$  (where  $\sigma$  is the standard deviation of the errors). Detailed information of clipping points can be found in [15].

In practice, one needs to estimate the standard deviation of the errors to calculate clipping points. Usually, a robust measure of scale is preferred for the standard deviation of  $e_i$ . For example, a common approach is to take  $\hat{\sigma} = \text{MAD} \cdot 1.4826$ , where  $\text{MAD} = \text{median}_i(|e_i - \text{median}_j(e_j)|)$  is the median absolute deviation.

Now, the weighted least-squares solution of (17) is

$$\hat{\mathbf{x}} = (\mathbf{N}^T \boldsymbol{\Omega} \mathbf{N})^{-1} \mathbf{N}^T \boldsymbol{\Omega} \mathbf{Y} \quad (24)$$

where  $\boldsymbol{\Omega} = \text{diag}\{w(e_1), \dots, w(e_n)\}$ , with the diagonal matrix  $\text{diag}(\cdot)$ . These steps are repeated until the state estimate converges to a stable value.

### C. IMM Estimator

From the previous section, EKF can only follow the true trajectory in the LOS environment; on the contrary, the REKF can cope with some NLOS interference by choosing a smaller clipping point for the price of losing performance in the LOS environment. It is affirmative that better results can be achieved if these two methods are combined [14].

The multiple model algorithm is based on the fact that the behavior of the MS cannot be characterized at all times by a single model. One of the schemes is called the generalized pseudo-Bayesian (GPB) method and another one is the IMM method. The general structure of these algorithms consists of more than one filter matched to different models. The IMM method is conceptually similar to the second-order GPB and performs nearly as well as the second-order GPB with less computations as the first-order GPB. Hence, the IMM method being a suboptimal hybrid filter is shown to achieve an excellent compromise between performance and complexity [16]. The detail of GPB is given in [17].

In this paper, we only focus on the IMM method. Two modes are considered in our case: LOS mode and NLOS mode. The EKF estimator is matched for tracking an MS for

the LOS case and the REKF estimator for the NLOS case. Since the REKF estimator is not matched for the LOS case, a redescending score function with smaller clipping points is chosen for the REKF estimator in order to efficiently alleviate the noise impact in NLOS situations.

The structure of the IMM algorithm consists of five components. These are mixing probability calculation, interaction, mode-matched filtering, mode probability update, and combination [18], shown in Fig. 3.

The algorithm is as follows.

- 1) *Calculation of the mixing probabilities ( $i, j = 1, 2$ ):*  
According to Bayes' formula

$$\mu_{k-1}^{i|j} = \frac{1}{\bar{c}_j} \pi_{ij} \mu_{k-1}^i \quad (25)$$

where the normalizing constants are

$$\bar{c}_j = \sum_i \pi_{ij} \mu_{k-1}^i \quad (26)$$

and  $\pi_{ij}$  is the transition probability from mode  $i$  to mode  $j$  and  $\mu_{k-1}^i$  is the probability of the  $i$ th mode at the time step  $k-1$ .

- 2) *Interaction ( $j = 1, 2$ ):*

In this step, the mixing initial conditions  $\hat{\mathbf{x}}_{k-1}^{0j}$  and  $\mathbf{P}_{k-1}^{0j}$  for each mode-matched filter are calculated in order to prevent from  $2^2$  parallel filtering as the second-order GPB [17]

$$\hat{\mathbf{x}}_{k-1}^{0j} = \sum_i \hat{\mathbf{x}}_{k-1}^i \mu_{k-1}^{i|j} \quad (27)$$

$$\tilde{\mathbf{x}}_{k-1}^{ij} = \hat{\mathbf{x}}_{k-1}^i - \hat{\mathbf{x}}_{k-1}^{0j} \quad (28)$$

$$\mathbf{P}_{k-1}^{0j} = \sum_i \mu_{k-1}^{i|j} \left\{ \mathbf{P}_{k-1}^i + \tilde{\mathbf{x}}_{k-1}^{ij} (\tilde{\mathbf{x}}_{k-1}^{ij})^T \right\}. \quad (29)$$

- 3) *Mode-matched extended Kalman filtering ( $j = 1, 2$ ):*

In this step, the two mixing state estimates and their corresponding covariances are the inputs of our two mode-matched filters: EKF and REKF.

Within the filtering, the likelihood functions corresponding to two filters are computed by

$$\Lambda_k^1 = \mathcal{N}(\mathbf{e}_k^1; 0, \mathbf{S}_{\text{LOS},k}) \quad (30)$$

$$\Lambda_k^2 = \mathcal{N}(\mathbf{e}_k^2; 0, \mathbf{S}_{\text{NLOS},k}) \quad (31)$$

where  $\mathbf{e}_k^1$  and  $\mathbf{e}_k^2$  being the innovations for Modes 1 and 2 are given by

$$\mathbf{e}_k^j = \mathbf{z}_k - h(\hat{\mathbf{x}}_{k|k-1}^{0j}), \quad j = 1, 2 \quad (32)$$

where  $\hat{\mathbf{x}}_{k|k-1}^{0j} = \mathbf{A} \hat{\mathbf{x}}_{k-1}^{0j}$ .

$\mathbf{S}_{\text{LOS},k}$  and  $\mathbf{S}_{\text{NLOS},k}$  are calculated according to the following equations:

$$\mathbf{S}_{\text{LOS},k} = \mathbf{H}_k^1 \mathbf{P}_{k|k-1}^{01} (\mathbf{H}_k^1)^T + \mathbf{R}_{\text{LOS},k} \quad (33)$$

$$\mathbf{S}_{\text{NLOS},k} = \mathbf{H}_k^2 \mathbf{P}_{k|k-1}^{02} (\mathbf{H}_k^2)^T + \mathbf{R}_{\text{NLOS},k} \quad (34)$$

Here, the multivariate normal probability density function is used as the likelihood function for both modes.

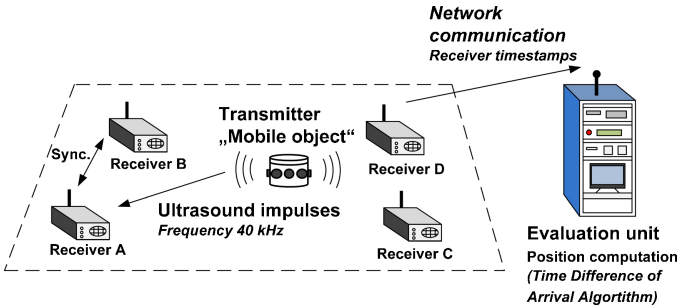


Fig. 4. Overview of the system.

4) *Mode probability update*( $j = 1, 2$ ):

In this step, the new mode probabilities are computed

$$\mu_k^j = \frac{1}{c} \Lambda_k^j \bar{c}_j \quad (35)$$

where the normalization constant for (35) is

$$c = \sum_j \Lambda_k^j \bar{c}_j \quad (36)$$

where  $\bar{c}_j$  is the expression from (26) and  $\Lambda_k^j$  is the likelihood computed in Step 3.

5) *Combination* ( $j = 1, 2$ ):

In this step, the combination of the estimates and corresponding covariances of two modes is executed according to the mixture equations given in (37) and (38). The combination result is only used for output purposes and is not the input for the next time step

$$\hat{\mathbf{x}}_k = \sum_j \hat{\mathbf{x}}_k^j \mu_k^j \quad (37)$$

$$\mathbf{P}_k = \sum_j \mu_k^j \left\{ \mathbf{P}_k^j + \hat{\mathbf{x}}_k^j (\hat{\mathbf{x}}_k^j)^T \right\} \quad (38)$$

where  $\hat{\mathbf{x}}_k^j$  is

$$\hat{\mathbf{x}}_k^j = \hat{\mathbf{x}}_k^j - \hat{\mathbf{x}}_k. \quad (39)$$

The derivation of the IMM algorithm is given in [17].

#### IV. ULTRASONIC SYSTEM

In the area of mobile robots or airplanes and miniature indoor blimps, localization systems with specific requirements are needed; however, most of the localization systems available are not able to fulfill those requirements due to their sizes, weights, or power consumptions [19]–[21]. In this paper, we have built an ultrasonic localization system, which has reduced hardware complexities on its MS side, a position update rate of more than 3 Hz, and a minimum ranging distance of 10 m.

The overview of our self-built ultrasonic localization system is shown in Fig. 4. The mobile transmitter is mounted on an MS and sends short ultrasound impulses to the receivers (BSs). The receivers determine the TOA of the impulses. An evaluation unit collects the timestamps and calculates the positions using the IMM estimator.

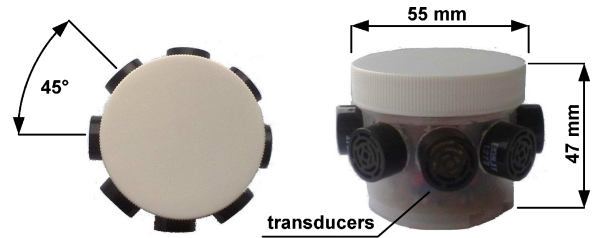


Fig. 5. 2-D isotropic ultrasound transmitter.

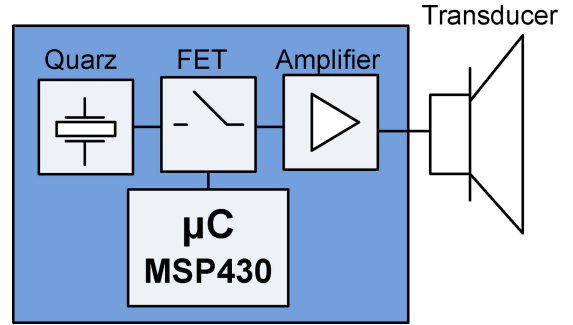


Fig. 6. Block diagram of the ultrasound transmitter.

##### A. Transmitter

A conventional ultrasonic transmitter is limited by the beam width. Ming *et al.* [22] presented a combination of two ultrasonic transducers to increase the beam width (factor 2) so that the coverage of the ultrasound localization system becomes wider. We developed a 2-D isotropic ultrasound transmitter with a beam width of 360°, which is shown in Fig. 5. The block diagram of the transmitter is given in Fig. 6. An MSP430 microcontroller generates 1-ms impulse per 300 ms with an ultrasound frequency of 40 kHz. For each ultrasound transducer, an amplifier is used to amplify the impulses to extend the transmitting distance.

The isotropic transmitter consists of an array of eight ultrasound transducers placed in a round body. The angle of aperture of one transducer is 45°. By using eight ultrasound transducers, the coverage range can be increased by a factor of 8. The 360° radiation pattern of our transmitter in the  $x-y$  plane is shown in Fig. 7.

##### B. Receiver

The receivers have fixed positions around the localization area. The receivers were developed to receive the ultrasonic signals and detect the arrival timestamps of the transmitted signals. Fig. 8 shows the developed ultrasound receiver with an envelope detector.

The sound signals were received by the ultrasound transducer. The incoming sound signals were filtered from a fourth-order bandpass filter and amplified by a factor of 300 to detect the 40 kHz signals (see Fig. 9). After filtering, the envelope of the original signal is produced with a half-wave rectifier. The envelope is digitized by a 12-bit analog-to-digital converter. The digital data are analyzed with the ATxmega128 microcontroller. The edge of the incoming signals was detected with a dynamic threshold. Over a time span of 30 ms,

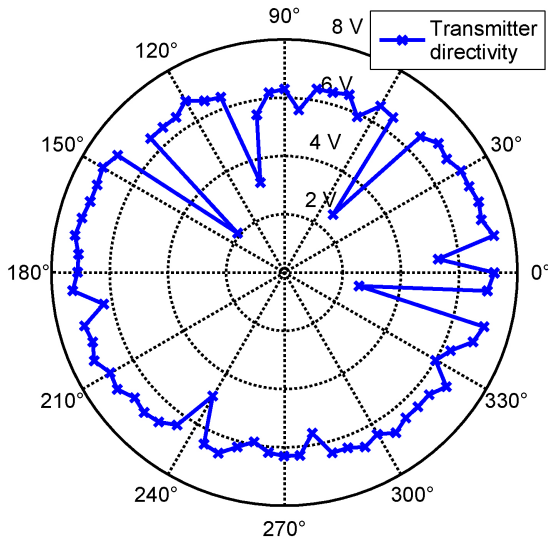
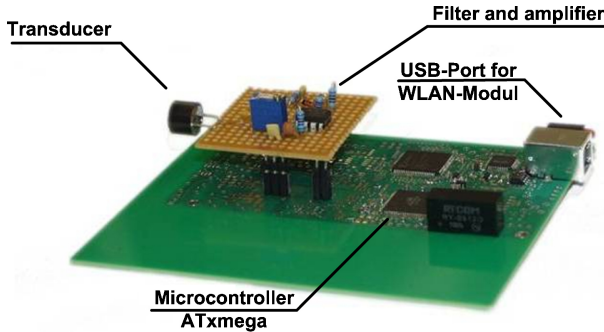
Fig. 7. Radiation pattern of the transmitter in the  $x$ - $y$  plane.

Fig. 8. Developed ultrasound receiver.

the incoming sound signals were averaged. The minimum amplitude of detected impulses should be at least ten times bigger than one of the average signal. Signals below this threshold were discarded.

To determine the arrival time of received sound impulses, a precise time synchronization is needed, as the accuracy of the localization system relies on how precise the synchronization between the receivers is. In this study, the receivers are connected together via a WLAN for communication. The connected receiver clients negotiate with one master receiver which acts as a time reference and other clients adjust their clocks to the master. The synchronization is achieved with a series of pings between master and slave via the user datagram protocol to get a good estimation of the RTT to the master. The time of slave is then corrected by using  $\frac{1}{2}$ RTT. Both time offset and clock drift between slave and master are obtained by a linear regression of the set of timestamps. The calculation is done by an adaption of the network time protocol algorithm. The implementation of synchronization can be found in [23]. A summary of the synchronization in wireless sensor networks is given in [24].

The phenomenon of multipath propagation, i.e., echoes from walls or objects, was encountered by issuing a dead time period and by using minimal signal length after every received signal. Fig. 10 shows received sound impulses. In

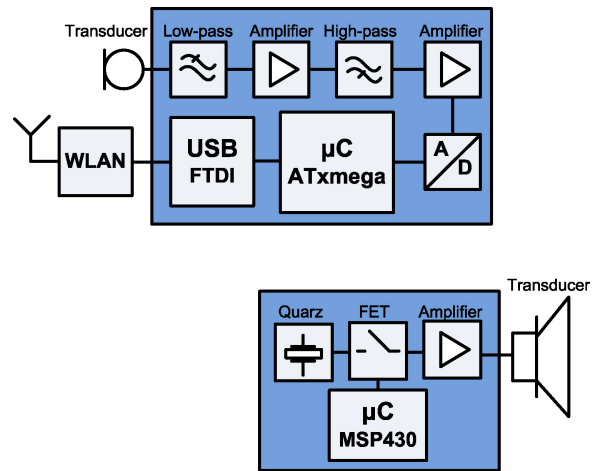


Fig. 9. Block diagram of the ultrasound receiver.

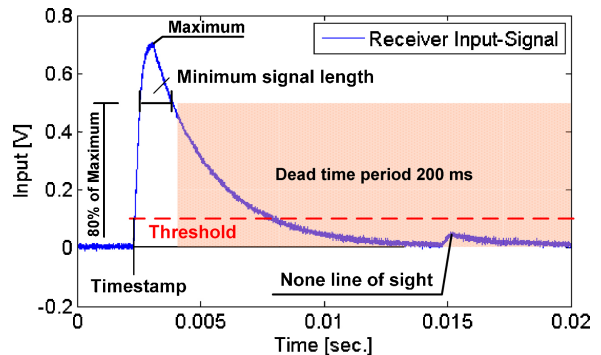


Fig. 10. Input of a received sound impulse.

our study, after the first peak, the microcontroller detects the length of signals (80% of the maximum amplitude) and generates a dead time period (200 ms) to fade out false sound signals from multipath propagation. Although Angrisani *et al.* introduced a Kalman filter-based estimation of the ultrasound to achieve a higher accuracy [25], the computational and power consumptions of this method are still high for our system.

### C. Distance Measurement Accuracy

According to (1), the distance between the MS and the  $i$ th BS  $D_i$  can be calculated by

$$\begin{aligned} D_i &= \sqrt{(x_{BS_i} - x_{MS})^2 + (y_{BS_i} - y_{MS})^2 + v_i} \\ &= v_{us} \times t_{BS_i}. \end{aligned} \quad (40)$$

The sound speed in air  $v_{us}$  can be calculated by the following equation:

$$v_{us} = 331.1 \text{ m/s} \sqrt{1 + \frac{\vartheta}{273.15^\circ\text{C}}}. \quad (41)$$

The speed of sound depends on the temperature  $\vartheta$  of the environment. At a temperature of  $25^\circ\text{C}$  the speed of sound is about 346 m/s.

In case of using sound waves instead of electromagnetic waves, the impact on the position accuracy from synchronization of the receiver decreases. Since the speed of sound is much lower than the speed of light, the same time delay

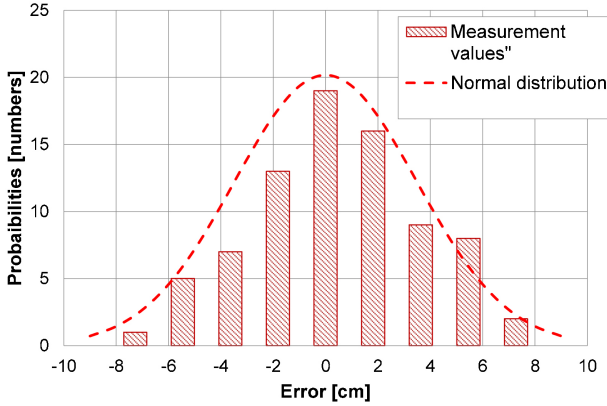


Fig. 11. Distance measurement of the ultrasound system.

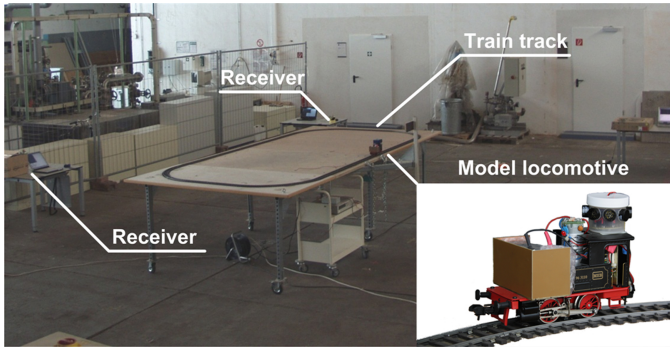


Fig. 12. Experiment environment with an ultrasonic transmitter fixed on a model locomotive [28].

caused by synchronization will result in much smaller position error. We have achieved a synchronization precision better than 0.1 ms with a 802.11 b/g Wi-Fi connection [26]. In this case, the theoretical maximum error of localization from synchronization is about 3.46 cm when the temperature is about 25 °C. The distance measurement accuracy between a transmitter and a receiver is shown in Fig. 11.

## V. EXPERIMENTAL RESULTS

To validate the absolute position accuracy as well as the system repeatability, a model railway is used. The track of the railway is about 1.75 m times 3.85 m of rectangular shape with rounded corners and has a length of 10.35 m. The track is placed in a rectangular measurement area of  $10 \times 12 \text{ m}^2$  within a factory building [27] and the ultrasonic transmitter is fixed on the model locomotive, which can be seen in Fig. 12. The speed of mode locomotive is about 0.2–0.3 m/s. The seven receivers are fixed around the track of the model railway as shown in Fig. 13.

During the experiment, the speed of ultrasound is about 343 m/s and the frequency of ultrasound is about 40 kHz. The time step duration  $dt$  for the position update is 0.3 s. Since the rail track is not always straight, smaller  $\mathbf{R}$  and bigger  $\mathbf{Q}$  are chosen in comparison to normal random walk. In this paper,  $\mathbf{Q}$  is chosen as 1 and  $\mathbf{R}_{\text{LOS}}$  is chosen as  $0.01 \cdot \mathbf{I}_{6 \times 6}$ .  $\mathbf{R}_{\text{NLOS}} = 2 \cdot \mathbf{R}_{\text{LOS}}$ . Since we have no preknowledge about the probabilities for two filter modes, the initial mode probability

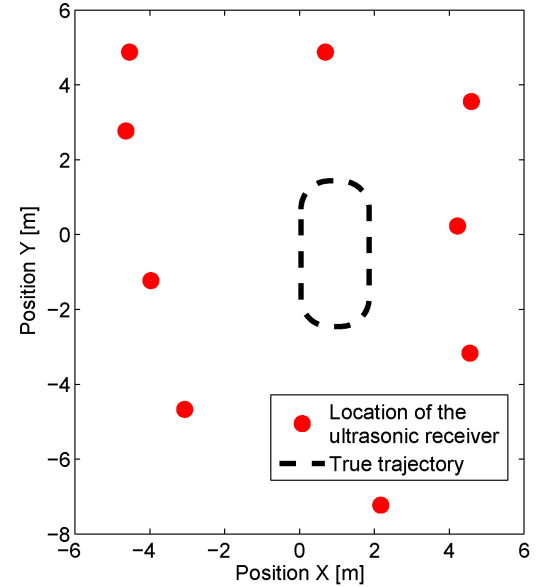


Fig. 13. Position of receivers and railway track.

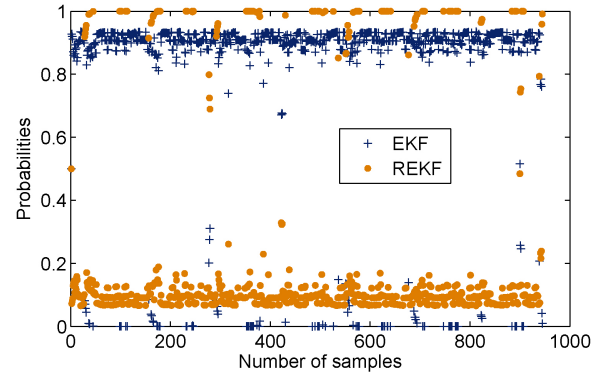


Fig. 14. Probability comparison of two modes inside the IMM estimator.

$\mu_0^i, i = 1, 2$ , is set as 0.5. For the general case, the transition probability matrix which contains  $\pi_{ij}, i, j = 1, 2$  is also set as

$$\begin{bmatrix} 0.5 & 0.5 \\ 0.5 & 0.5 \end{bmatrix}.$$

Since the path between transmitter and receiver can be blocked due to obstacles or bad transmission angles, the strength of NLOS interference is not only estimated by the NLOS propagation, but also assessed by the number of invalid receivers, which receive no ultrasonic signal from the transmitter. When less measurements are being received, the possibility to correct measurement noise by using other measurements is less and more measurement noise remains, which requires larger  $\mathbf{R}$  during the filtering.

It can be seen from Fig. 14 that the probability of EKF mode is much higher than one of the REKF mode during most of the time. Due to the fact that less NLOS interferences exist, the receivers are able to provide enough measurement information to track the model locomotive correctly. During the time, the IMM estimator is more like an EKF estimator.

At the same time, the REKF estimator performs much worse than the EKF estimator as shown in Figs. 15 and 16 since the

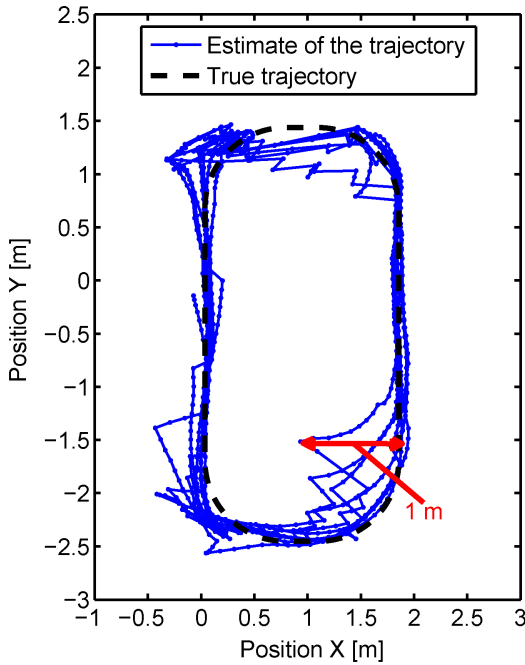


Fig. 15. Railway track estimated by EKF.

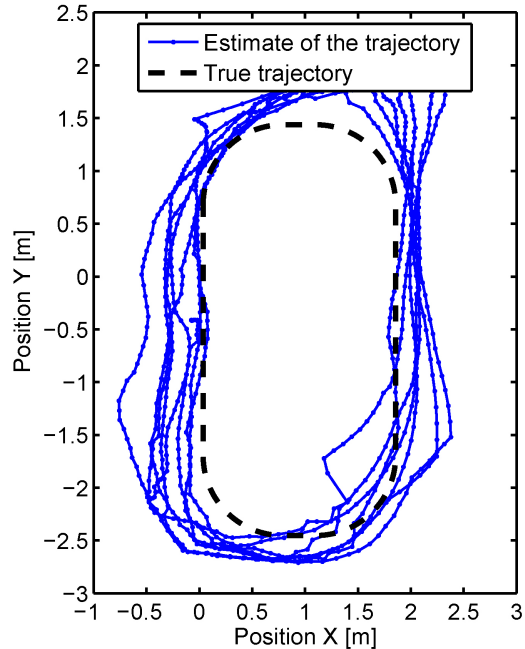


Fig. 16. Railway track estimated by REKF.

REKF estimator is tuned to handle NLOS interference with a large  $\mathbf{R}$ .

However, when NLOS interference becomes large, i.e., two receivers keep experiencing NLOS propagation and become invalid continually for some time or more than two receivers experience NLOS propagation and become invalid, the probability of REKF mode becomes higher, as can be seen in Fig. 17. During this time period, the IMM estimator functions like an REKF estimator. The EKF estimator being tuned to handle the LOS situation no longer tracks the true trajectory

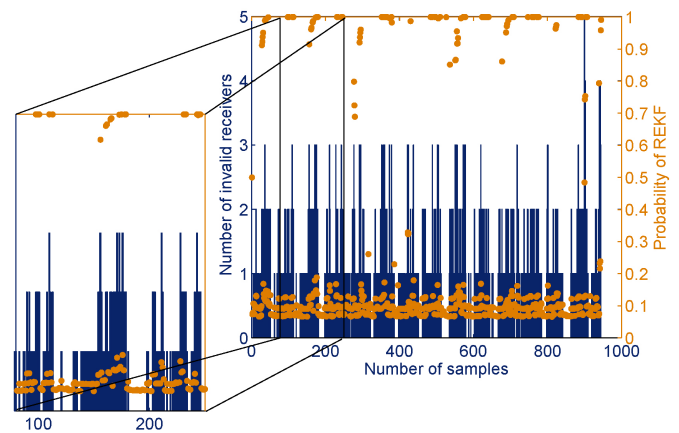


Fig. 17. Number of the invalid receivers versus probabilities of REKF modes.

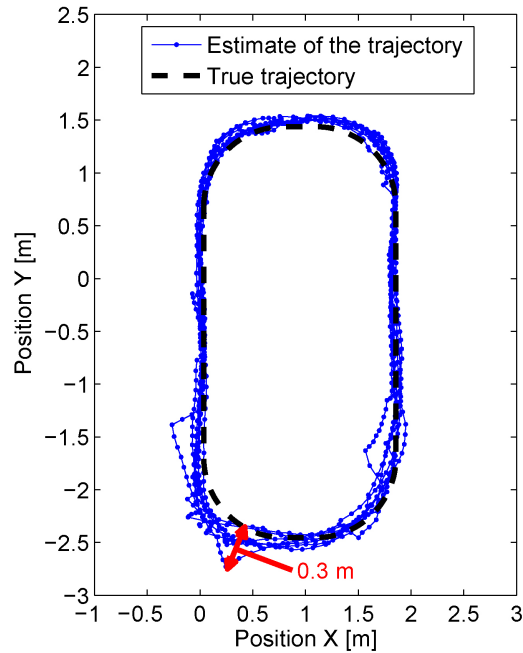


Fig. 18. Railway track estimated by IMM.

and incorrect estimations occur around the railway corners, as shown in Fig. 15.

In comparison to the EKF estimator or the REKF estimator, the IMM estimator is however able to switch between the internal modes to take the advantages of both modes; hence, it provides a robust and stable position estimation in both LOS and NLOS environments, as shown in Fig. 18.

In our previous study, the MS tracking using an electromagnetic system from Nanotron Technologies<sup>1</sup> was presented. This system works with TOA/TDOA measurement at 2.4 GHz and uses the chip spread spectrum (CSS) modulation scheme. The CSS modulation is based on the so-called chirp impulses, a wobbled frequency impulse, which sweeps in a short time span a predefined frequency band. To determine the distance between MS and BSs, the ranging methodology symmetrical

<sup>1</sup><http://www.nanotron.com>

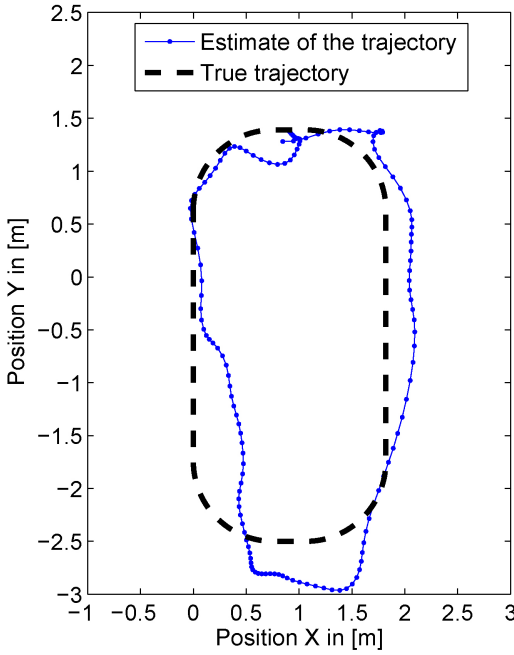


Fig. 19. Nanotron localization result using EKF [29].

double-sided two-way ranging is used by the Nanotron system. More information of this paper can be found in [29]. The result of our previous study is shown in Fig. 19. It can be seen clearly that our new ultrasonic localization system delivered much better positioning solution than the Nanotron system.

## VI. CONCLUSION

This paper presented a wireless network infrastructure-based indoor localization system using an ultrasonic system for obtaining TDOA measurements and the IMM estimator for determining accurate positioning. Compared with the conventional radio signal, the ultrasonic signal is more robust and stable when deployed in noisy environments [29]; the recording of TOA is thus more accurate. The IMM estimator runs EKF and REKF estimators simultaneously and combines their results by calculating the probabilities of each estimator; therefore, localization with high accuracy can be achieved in both LOS and NLOS noise scenarios. The experimental results showed that our localization system was able to track the true trajectory of a model locomotive and outperformed the Nanotron system.

However, due to the short transmission distance between the transmitter and the receiver, our current system is only for small area localization. Future work will focus on enlarging the transmission distance and adding an inertial measurement unit for assistance to obtain the relative position information [30]–[33] so that the MS can still be localized even if the MS is outside the ultrasonic signal range.

## ACKNOWLEDGMENT

The authors would like to thank J. Wendeberg and M. Sippel for building the ethernet communication and creating the railway experiment.

## REFERENCES

- [1] R. Zhang, F. Höflinger, and L. M. Reindl, “TDOA based localization using interacting multiple model estimator and ultrasonic transmitter/receiver,” in *Proc. IEEE 9th Int. Multi-Conf. Syst., Signals Devices*, Mar. 2012, pp. 1–6.
- [2] F. Gustafsson and F. Gunnarsson, “Mobile positioning using wireless networks: Possibilities and fundamental limitations based on available wireless network measurements,” *IEEE Signal Process. Mag.*, vol. 22, no. 4, pp. 41–53, Jul. 2005.
- [3] Nikon Metrology NV. (2010). *iSpace, Large Volume Metrology, Tracking and Positioning* [Online]. Available: [http://www.nikonmetrology.com/en\\_EU/content/download/10938/219240/version/2/file/iSpace\\_EN.pdf](http://www.nikonmetrology.com/en_EU/content/download/10938/219240/version/2/file/iSpace_EN.pdf)
- [4] Symeo GmbH. (2008). *LPR-2D Positionserfassung von Kränen und Fahrzeugen zur Warenverfolgung* [Online]. Available: [http://www.symeo.com/cms/upload/PDF/Datenblatt\\_LPR-2D.pdf](http://www.symeo.com/cms/upload/PDF/Datenblatt_LPR-2D.pdf)
- [5] P. Bahl and V. Padmanabhan, “Radar: An in-building RF-based user location and tracking system,” in *Proc. 19th Annu. Joint Conf. IEEE Comput. Commun. Soc.*, Mar. 2000, pp. 775–784.
- [6] K. Draguñas and K. Borre, “Indoor multipath mitigation,” in *Proc. Int. Conf. IPIN*, Sep. 2010, pp. 1–7.
- [7] N. B. Priyantha, “The cricket indoor location system,” Ph.D. dissertation, Dept. Elect. Eng. Comput. Sci., Massachusetts Inst. Technol., Cambridge, MA, USA, 2005.
- [8] N. B. Priyantha, A. Chakraborty, and H. Balakrishnan, “The cricket location-support system,” in *Proc. 6th ACM MOBICOM*, 2000, pp. 32–43.
- [9] M. Najar and J. Vidal, “Kalman tracking based on TDOA for UMTS mobile location,” in *Proc. 12th IEEE Int. Symp. Pers., Indoor Mobile Radio Commun.*, vol. 1, Sep. 2001, pp. B45–B49.
- [10] A. Muhammad, “Evaluation of TDOA techniques for position location in CDMA systems,” M.S. thesis, Virginia Polytechnic Inst. State Univ., Blacksburg, VA, USA, 1997.
- [11] G. Welch and G. Bishop, “An introduction to the Kalman filter,” Univ. North Carolina Chapel Hill, Chapel Hill, NC, USA, Tech. Rep. TR 95-041, Feb. 2001.
- [12] A. Francine, “Tracking of a mobile station in non-line-of-sight environments using network infrastructure,” M.S. thesis, Dept. Elect. Eng. Inf. Technol., Tech. Univ. Darmstadt, Darmstadt, Germany, 2008.
- [13] T. Perala and R. Piche, “Robust extended Kalman filtering in hybrid positioning applications,” in *Proc. 4th Workshop Position., Navigat. Commun.*, Mar. 2007, pp. 55–63.
- [14] R. Zhang, “Wireless network-based positioning of a mobile station in non-line-of-sight environment,” M.S. thesis, Dept. Elect. Eng. Inf. Technol., TU Darmstadt, Darmstadt, Germany, 2009.
- [15] J. Fox and S. Weisberg, in *An R Companion to Applied Regression*, 2nd ed. Thousand Oaks, CA, USA: Sage, 2011.
- [16] E. Mazor, A. Averbuch, Y. Bar-Shalom, and J. Dayan, “Interacting multiple model methods in target tracking: A survey,” *IEEE Trans. Aerosp. Electron. Syst.*, vol. 34, no. 1, pp. 103–123, Jan. 1998.
- [17] Y. Bar-Shalom, X. Li, and T. Kirubarajan, *Estimation With Applications to Tracking and Navigation, Theory Algorithms and Software*. New York, NY, USA: Wiley, 2001.
- [18] C. Fritzsche, U. Hammes, A. Klein, and A. M. Zoubir, “Robust mobile terminal tracking in NLOS environments using interacting multiple model algorithm,” in *Proc. IEEE Int. Conf. Acoust., Speech Signal Process.*, Apr. 2009, pp. 3049–3052.
- [19] J. Müller, A. Rottmann, L. Reindl, and W. Burgard, “A probabilistic sonar sensor model for robust localization of a small-size blimp in indoor environments using a particle filter,” in *Proc. IEEE Int. Conf. Robot. Autom.*, May 2009, pp. 3589–3594.
- [20] R. Woods, S. Avadhanula, E. Steltz, M. Seeman, J. Entwistle, A. Bachrach, G. Barrows, S. Sanders, and R. Fearing, “An autonomous palm-sized gliding micro air vehicle,” in *Proc. IEEE Robot. Autom. Mag.*, vol. 14, no. 2, pp. 82–91, Jun. 2007.
- [21] J. Eckert, R. German, and F. Dressler, “An indoor localization framework for four-rotor flying robots using low-power sensor nodes,” *IEEE Trans. Instrum. Meas.*, vol. 60, no. 2, pp. 336–344, Feb. 2011.
- [22] Y. Ming, S. L. Hill, and J.O. Gray, “Localization of plane reflectors using a wide-beamwidth ultrasound transducer arrangement,” *IEEE Trans. Instrum. Meas.*, vol. 46, no. 3, pp. 711–716, Jun. 1997.
- [23] J. Wendeberg, “Laufzeitbasierte Schallortung mit unbekannten Sender- und Empfängerpositionen,” M.S. thesis, Dept. Comput. Sci., Univ. of Freiburg, Freiburg, Germany, 2009.

- [24] B. Sundararaman, U. Buy, and A. Kshemkalyani, "Clock synchronization for wireless sensor networks: A survey," *Ad Hoc Netw.*, vol. 3, no. 3, pp. 281–323, 2005.
- [25] L. Angrisani, A. Baccagalupi, and R. S. Lo Moriello, "A measurement method based on Kalman filtering for ultrasonic time-of-flight estimation," *IEEE Trans. Instrum. Meas.*, vol. 55, no. 2, pp. 442–448, Apr. 2006.
- [26] T. Janson, C. Schindelhauer, and J. Wendeberg, "Self-localization based on ambient signals," in *Proc. 6th Int. Workshop Algorithms Sensor Syst., Wireless Ad Hoc Netw. Auton. Mobile Entities*, 2010, pp. 176–188.
- [27] M. Sippel, "Localization of mobile objects with embedded microsystems," Ph.D. dissertation, Dept. Microsyst. Eng., Albert-Ludwigs-Univ. Freiburg, Freiburg, Germany, 2010.
- [28] J. Wendeberg, F. Höflinger, C. Schindelhauer, and L. Reindl, "Anchor-free TDOA self-localization," in *Proc. Int. Conf. Indoor Position. Indoor Navigat.*, Sep. 2011, pp. 1–10.
- [29] F. Höflinger, R. Zhang, and L. M. Reindl, "Wireless access to numerous destinations (WAND)-pointer for museums," in *Proc. Int. Conf. Indoor Position. Indoor Navigat.*, Sep. 2011, pp. 294–297.
- [30] R. Zhang and L. M. Reindl, "Pedestrian motion based inertial sensor fusion by a modified complementary separate bias Kalman filter," in *Proc. IEEE Sens. Appl. Symp.*, Feb. 2011, pp. 209–213.
- [31] X. Yun, J. Calusdian, E. R. Bachmann, and R. B. McGhee, "Estimation of human foot motion during normal walking using inertial and magnetic sensor measurements," *IEEE Trans. Instrum. Meas.*, vol. 61, no. 7, pp. 2059–2072, Jul. 2012.
- [32] A. R. Jiménez, F. Seco, J. C. Prieto, and J. Guevara, "Accurate pedestrian indoor navigation by tightly coupling foot-mounted IMU and RFID measurements," *IEEE Trans. Instrum. Meas.*, vol. 61, no. 1, pp. 178–189, Jan. 2012.
- [33] C. Tsai, "A localization system of a mobile robot by fusing dead-reckoning and ultrasonic measurements," *IEEE Trans. Instrum. Meas.*, vol. 47, no. 5, pp. 1399–1404, Oct. 1998.

**Rui Zhang** received the B.Sc. degree from the Beijing University of Aeronautics and Astronautics, Beijing, China, in July 2006, and the M.Sc. degree from the Institute of Telecommunications, Darmstadt University of Technology, Darmstadt, Germany, in May 2009. Since December 2009, he has been pursuing the Ph.D. degree at the Laboratory for Electrical Instrumentation, Institute of Microsystem Technology, Albert-Ludwigs University of Freiburg, Freiburg, Germany. His Ph.D. research focuses on indoor localization technologies. His current research interests include wireless infrastructure-based localization, inertial sensor-based localization, and human movement monitoring and classification.

Mr. Zhang was awarded the Siemens Master Program scholarship at the Beijing University of Aeronautics and Astronautics.

**Fabian Höflinger** received the B.Sc. degree in automation engineering from the University of Applied Sciences, Friedrichshafen, Germany, and the Master's degree in automation and energy systems from the Mannheim University of Applied Sciences, Mannheim, Germany, in 2007. He is currently pursuing the Ph.D. degree at the Albert-Ludwigs University of Freiburg, Freiburg, Germany.

While pursuing the B.Sc. degree, he was at Junghans Feinwerktechnik where he developed components for telemetric systems. While pursuing the Master's degree at the University of Applied Sciences, he developed inductive electronic components for programmable fuses. From 2007 to 2010, he was employed at a company for telemetric systems, where he was involved in research on inductive measurement and signal transformation. Since May 2010, he has been with the Laboratory for Electrical Instrumentation, Institute of Microsystem Technology, Albert-Ludwigs University of Freiburg.

**Leonhard Reindl** (M'XX) received the Diploma degree in physics from the Technical University of Munich, Munich, Germany, in 1985, and the Dr.Sci.Techn. degree from the Vienna University of Technology, Vienna, Austria, in 1997.

In 1985, he joined the Surface Acoustic Wave (SAW) Department, Siemens Corporate Technology Division, Munich, Germany, where he contributed to the development of SAW devices for signal processing and matched filtering in radio communications, radar systems, SAW-based identification marks, and wireless passive SAW-based sensors. In 1999, he joined the Institute of Electrical Information Technology, Clausthal University of Technology. In May 2003, he became a Full Professor in electrical instrumentation at the Institute for Microsystem Technology, Albert-Ludwigs University of Freiburg, Freiburg, Germany. He holds 45 patents on SAW devices and wireless passive sensor systems and has authored or co-authored more than 250 papers in this field. His current research interests include wireless sensor systems, energy harvesting systems, local positioning systems, and search and rescue systems for people buried in disasters.

Dr. Reindl is a member of the Technical Program Committees of the IEEE Frequency Control Symposium, the IEEE Ultrasonic Symposium, Eurosensors, Sensors, and of the German biannual Symposium "Sensoren und Messsysteme." He was an Elected Member of the AdCom of the IEEE Ultrasonics, Ferroelectrics, and Frequency Control Society from 2005 to 2007 and from 2010 to 2012.